المجلة الليبية للدراسات الأكاديمية المعاصرة (Libyan Journal of Contemporary Academic Studies)
LJCAS, eISSN: 5970-3005
Volume 3, Issue 2 (Part II), 2025, Pages: 124-129

Study physics structure of CdTe solar cell for PV applications

G. E. A. Muftah *
Physics Department, Faculty of Science, Bani Waleed University, Bani Waleed, Libya
*Corresponding author: muftah-geam4676@hotmail.com

دراسة البنية الفيزيائية لخلية شمسية من كادميوم تيلورايد (CdTe) لتطبيقات الطاقة الكهروضوئية

جعفر الصيد عوض *
قسم الفيزياء، كلية العلوم، جامعة بني وليد، بني وليد، ليبيا

Received: 12-09-2025; **Accepted:** 28-11-2025; **Published:** 13-12-2025

Abstract:
The objective of this research is to investigate CdTe structures using XRD technique in order to improve scientific understanding and enhance the efficiency further. The CdTe was prepared at different voltage between 655 to 695 mV vs SCE by electrodeposition technique. The effect of deposition voltage on bulk structural properties was investigated before and after heat treatment. The max intensive XRD pattern for all growth voltages was dominated by reflections from the (111) plane. The maximum intensity peak height was noticed from layers growth at 695 mV vs SCE indicating high crystallisation of CdTe. From which the physics structure of the material was studied.

Keywords: CdTe solar cell, XRD technique, Electrodeposition, Crystallinity, Deposition voltage.

الملخص :
يهدف هذا البحث إلى دراسة بنية مركب كادميوم تيلورايد (CdTe) باستخدام تقنية حيود الأشعة السينية (XRD) بهدف تعزيز الفهم العلمي وتحسين الكفاءة. تم تحضير CdTe عند جهود ترسيب مختلفة بين 655 و695 ملي فولت مقابل القطب المرجعي SCE باستخدام تقنية الترسيب الكهربي. جرى تحليل تأثير جهد الترسيب على الخصائص البنيوية قبل وبعد المعالجة الحرارية. أظهرت أنماط حيود الأشعة السينية أن الانعكاسات من المستوى (111) هي المهيمنة عند جميع جهود النمو، مع تسجيل أعلى شدة للقمم عند جهد 695 ملي فولت مقابل SCE، مما يشير إلى درجة عالية من التبلور لمركب CdTe، ومن خلالها تمت دراسة البنية الفيزيائية للمادة.

الكلمات المفتاحية: خلية شمسية كادميوم تيلورايد، تقنية حيود الأشعة السينية، الترسيب الكهربي، التبلور، جهد الترسيب.

Introduction

Second generation solar cells are based on thin film materials. One methods of the solar cell manufactory is electrodeposition, where the material is directly deposited onto a conducting glass substrate. This method has several advantages: the manufacturing process is fast, deposition is easy, and the cost is low. However, this method suffers from poor light conversion efficiency due to the polycrystalline structure of materials. This leads to the fabrication of larger module areas, and hence an increased cost. The research in solar cells is currently focused on $CuInGaSe_2$, CdTe, and $CuInTe_2$ semiconductor materials. CdTe show the highest conversion efficiencies of about 22% for lab scale devices, measured under the global AM 1.5 conditions [1,2,3]. XRD is one of the most important techniques used to characterise the structure of CdTe materials and to help identifying the phases of the semiconductor material [4].

Experimental Aspect

x-ray crystallography is employed in order to characterize CdTe structure [5]. In this manner Bragg's law is of course has to be engaged. It says that the difference between two constructive interference has to be equal to a wavelength or multiples of wavelengths.

$$2d.\sin\theta = n\lambda \qquad \text{(Bragg Equation)} \qquad (1)$$

λ is the wavelength of x-rays incident on a crystal, n is an integer number, , d is the inter planer distance, θ is the diffraction angle.

Copyright: © 2025 by the authors. Submitted for possible open access publication under the terms and conditions of the Creative Commons Attribution (CC BY) license (https://creativecommons.org/licenses/by/4.0/).

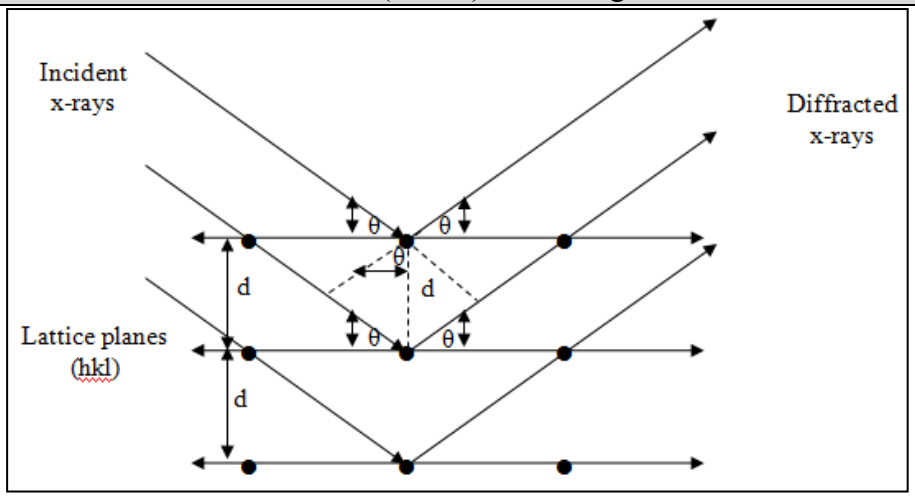

Figure 1: Graphic illustration showing the principle of x-ray diffraction by CdTe planes.

Figure 2 shows schematically x-ray diffraction machine that was used to test CdTe thin film solar cells. The CdTe sample fix at particular position as show in the figure. So when x-ray falls on the sample, it will be diffracted in all direction. only contractive interference will satisfy Bragg's law and we will have pecks intensity at a particular angles. This can be perform by continuously varying θ.

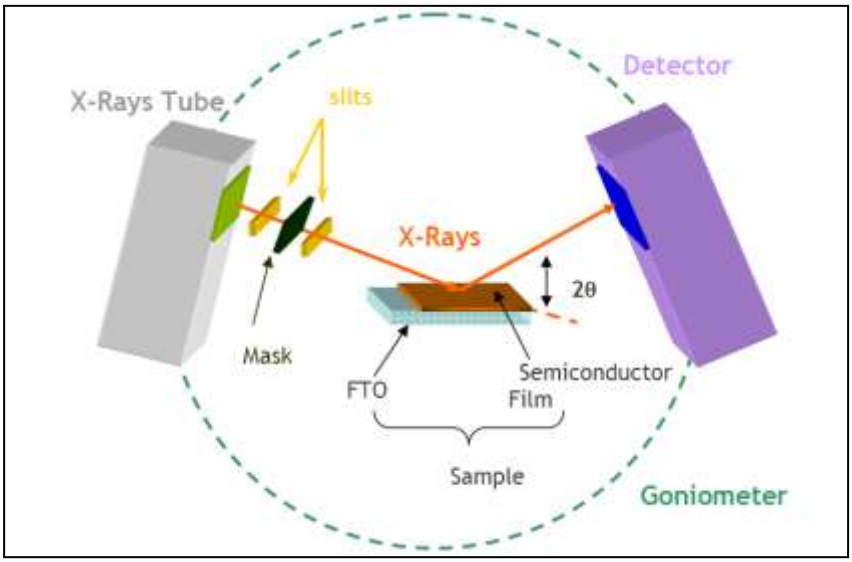

Figure 2: X-Ray diffraction technique.

The output result has to be plotted. It will come out with a collection of peaks. The intensity of x-ray counts versus diffraction angle 2θ. These peaks and their intensities have to be studied in order to define CdTe unit cells. The full width at half maximum (FWHM) of the individual x-ray peaks gives information on the grain size (D) using equation (2). Examination of the peak intensities and their positions gives information on CdTe Layer such as preferred orientation, inter planer distance and the atomic arrangement within the crystalline lattice [1].

$$D = \frac{0.89\lambda}{b\cos\theta} \qquad (2)$$

D is grain size (nm), λ is wavelength of incident radiation (Å), b is FWHM of the diffracted lines (radians) and θ is angle of diffraction (°).
The lattice parameters can be figure out from the equations 3, 4 and 5[1].

For cubic structure: $a=b=c$, $\alpha=\beta=\gamma=90°$

$$\frac{1}{d^2} = \frac{h^2+k^2+l^2}{a^2} \qquad (3)$$

Copyright: © 2025 by the authors. Submitted for possible open access publication under the terms and conditions of the Creative Commons Attribution (CC BY) license (https://creativecommons.org/licenses/by/4.0/).

For tetragonal structure: a=b≠c, α=β=γ=90°

$$\frac{1}{d^2} = \frac{h^2 + k^2}{a^2} + \frac{l^2}{c^2} \quad (4)$$

For hexagonal structure: a=b≠c, α=β=90° γ =120°

$$\frac{1}{d^2} = \frac{4}{3}\left(\frac{h^2 + k^2 + hk}{a^2}\right) + \frac{l^2}{c^2} \quad (5)$$

d is the inter planer distance (nm), (hkl) are Miller Indices and a, b and c are lattice parameters (nm).
Philips X-Pert Pro-diffractmeter was used for x-ray diffraction measurements. A Cu target with a tungsten filament was employed to emit characteristic Kα photons with a wavelength of λ=1.5418 Å.

CdTe films were cathodically deposited on CdS/TCO/Glass superstrate samples masked with polyimide tape using a three electrode configuration. The annealed superstrate CdS surface was etched in NH4OH. The anode (counter electrode) was formed from a Cd sheet (high purity) with the same dimensions as the CdS electrode with a Cd wire (high purity) additionally used as the reference electrode. The species concentrations and deposition conditions were an aqueous solution containing 0.8 M cadmium sulphate (3CdSO4.8H2O) and 50 ppm tellurium dioxide (TeO2) with a purity of 5N (99.999%). The pH value was set to 2.0 using high-purity sulphuric acid (H2SO4). As the deposition is dependent of the substrate condition, the deposition parameters were re-established. The annealing conditions were 350 for 20 mins in air.
CdTe is co-deposited in an aqueous electrolyte of Cd2+ and a very low concentration of HTeO2+. The initial tasks undertaken were to optimize the deposition temperature, pH of the electrolyte, stirring rate, complexing agents and nitrogen purging during deposition on CdTe layers. This cathodic deposition of CdTe is slow and usually proceeds along a two-dimensional or three-dimensional nucleation and growth mechanism, depending on the substrate surface and its condition. For an effectively low-cost process, it would be essential to improve the deposition rate by the optimisation of the above parameters and the feeding mechanism of constituent species (Cd2+ and HTeO2+) in the electrolyte as the rate of deposition of CdTe used previously was ~200 nm/hour.

Result and discussion
Linear Sweep Voltammetry (LSV) is another important guide to understand the chemical reactions taking place and is used to establish suitable deposition conditions. Collected data are plotted with current density against voltage as shown in figure 3. The plots of current density against cathodic voltage with different bath parameters give different shaped voltammograms, indicating the range of different chemical reactions. Some extrapolation of both the straight line and rising portion of a current versus cathodic voltage leads to estimate as to where and what compounds are being deposited particularly when read in conjunction with the potential-pH diagram. It is possible then to work out what compounds are formed at a particular deposition voltage and pH. Therefore it has been utilized to choose the optimal deposition of CdTe range. As can be seen from the figure, the most suitable range growth voltage is between 655 and 695 mV vs SCE vs SCE.

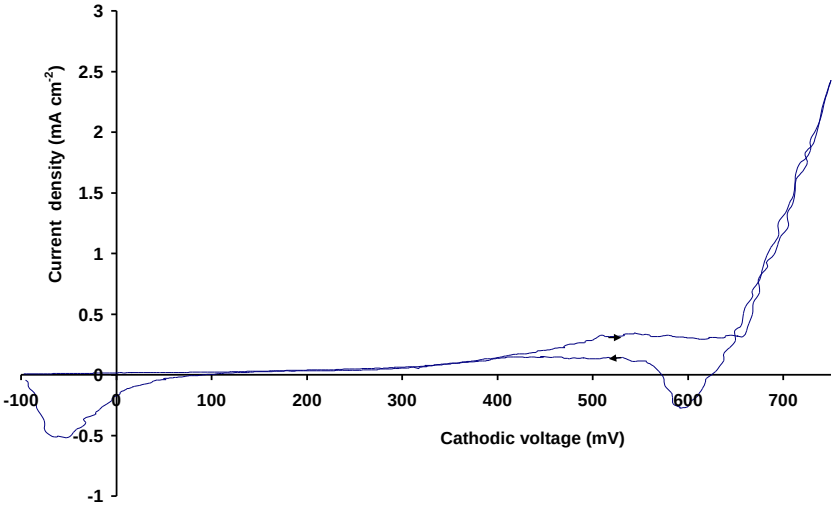

Figure 3: linear sweep voltage of CdTe solution. The solution was included 0.86 M $3CdSO_3.8H_2O$ and 50 ppm-TeO_2 , at 70°C. The direction of potential sweep is indicated by arrows.

Copyright: © 2025 by the authors. Submitted for possible open access publication under the terms and conditions of the Creative Commons Attribution (CC BY) license (https://creativecommons.org/licenses/by/4.0/).

In order to identify the crystalline nature and phase content of the electrodeposited layer as a function of deposition voltage, XRD measurements were performed on both as-deposited and annealed CdTe layers. Figure 4 and 5 illustrate the XRD spectra for as-deposited CdTe and annealed samples respectively. The films were growth at different voltage 655, 665, 675, 685 and 695 mV vs SCE and heated for 20 minutes at 350°C. it can be figure out that the major preferential reflection was from the (111) plane for all growth voltage and several researchers observed similar result [6,7]. The analysis showed that the structure of CdTe was cubic CdTe, which coincide with some authors in the literatures [8,9,10]. The intensity of the peak height increases with an increase in the deposition cathodic voltage. The maximum intensity peak height was observed from layers deposited at 695 mV vs SCE and the minimum intensity peak height was detected from layers deposited at 655 mV vs SCE for both as-deposited and annealed samples.

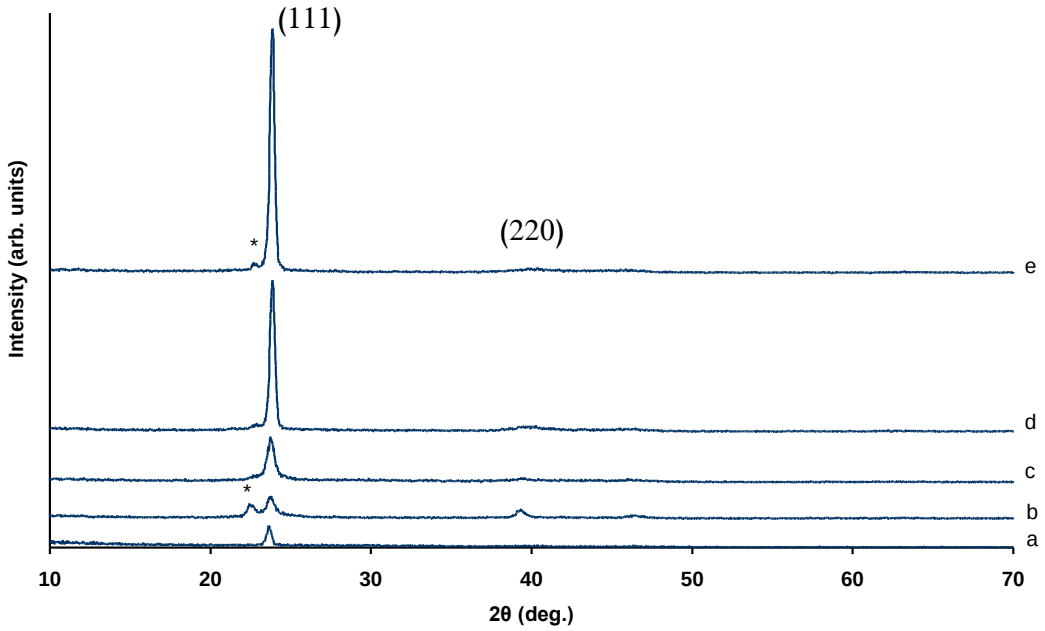

Figure 4: Typical XRD spectra of CdTe deposited at (a) 655, (b) 665, (c) 675, (d) 685 and (e) 695 mV vs SCE. The peak arising from the Te or TeO_2 is indicated by an asterisk (*).

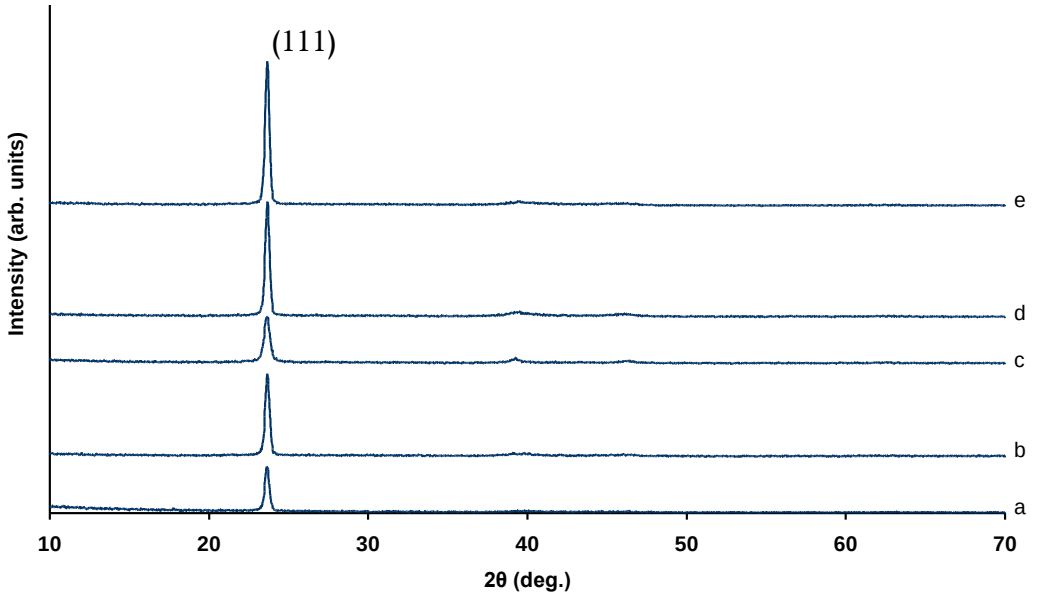

Figure 5: Typical XRD spectra of CdTe growth at (a) 655, (b) 665, (c) 675, (d) 685 and (e) 695 mV vs SCE and heated at 350°C for 20 mins. Excess Te or TeO_2 phases have been removed during heat treatment process.

Moreover, the change of deposition voltage towards more negative voltages gave more intense and sharp preferential reflection peaks indicating a better crystalline material with a chalcopyrite structure. In contrast the layers that were deposited at low cathodic voltages present broader widths indicating that the layers are becoming less crystalline. The layer deposited at 665 and 695 mV vs SCE showed an additional reflection related to Te or

Copyright: © 2025 by the authors. Submitted for possible open access publication under the terms and conditions of the Creative Commons Attribution (CC BY) license (https://creativecommons.org/licenses/by/4.0/).

TeO_2 which disappeared after annealing.
The data related to extra reflection was analyzed and presented in Table 1.

Table 1: The data related to extra reflection for layers deposited at 665 and 695 mV vs SCE , arising from Te or TeO_2.

Growth Voltage (mV) vs SCE	2θ (Observed)	2θ (Standard)	
		Te	TeO_2
665	22.49	23.03	22.92
695	22.79		

Table 2 shows peak position, FWHM and grain size of as-deposited layers as a function of growth voltage. In order to keep the thickness constant, the layers were deposited keeping the electric charge (Q=it) approximately constant. The grain size was calculated using the Scherrer equation. As can be seen from the Table , there is a variation in the FWHM and grain size; the layers deposited at 675 mV vs SCE show the smallest grain size and largest FWHM, while the CdTe layers deposited at 695 mV vs SCE present the largest grain size and smallest FWHM. This variation in intensity, FWHM and grain size from the as-deposited layers are due to changes in the composition of the CdTe layers, which are influenced by the growth voltage and Te concentration in the solution.

Table 2: Peak position, FWHM and grain size versus growth voltage for as-deposited CdTe layers.

Growth Voltage (mV) vs SCE	2θ (deg.)	FWHM (deg.)	Grain size (nm)
655	23.68	0.59	13.5
665	23.74	0.61	13.1
675	23.79	0.90	8.92
685	23.88	0.39	20.5
695	23.88	0.34	23.5

Peak position, FWHM and grain size of annealed layers as a function of deposition voltage are presented in Table 3. Similar to as-deposited layers, the layer deposited at 675 mV vs SCE shows the largest FHWM and smallest grain size and the layer deposited at 695 mV vs SCE presents the smallest FHWM and largest grain size, indicating the best crystalline CdTe comes from layers deposited at 695 mV vs SCE. Considering the major reflection peak related to the (111) plane at cathodic voltage 695 mV SCE, the lattice parameters were calculated using the cubic d-spacing equation, giving a=6.50 Å which is close to standard value of a=6.482 Å. The XRD data for as-deposited and annealed CdTe layers was investigated using standard data obtained from the online Deresbury Chemical Database Service [11].

Table 3: Peak position, FWHM and grain size versus growth voltage for annealed CdTe layers.

Deposition Voltage (mV) vs SCE	2θ (deg.)	FHWM (deg.)	Grain size (nm)
655	23.68	0.34	23.5
665	23.66	0.34	23.5
675	23.68	0.46	17.3
685	23.68	0.35	23.5
695	23.68	0.31	25.8

Figure 6 presents the variation of (111) peak height versus growth voltage for as-growth and annealed CdTe layers. It can be seen from the figure that there is a trend with an increase in the (111) peak height with increase in growth voltage, reaching a maximum values for layer deposited at 695 mV vs SCE. The improvement in the (111) peak height after annealing process was observed for all layers, except for layers deposited at higher voltages 690, 695 and 700 mV vs SCE. The decrease in the (111) peak height after annealing has been observed by D. Lincot's group (C. Leliller at al) [12] who reports an efficiency of 6%. The layers deposited at voltages greater than 695 mV vs SCE contained Cd-dendrites and therefore started to peel off.
These results lead to a very important conclusion which as follows. At lower cathodic voltages, the layers include Te/TeO_2 phases as expected, but after heat treatment, Te/TeO_2 sublimes leaving stoichiometric CdTe. Therefore, an improvement of crystallinity is observed for growth at low cathodic voltages. However, when the growth voltage is above 690 mV vs SCE, the as deposited layer seems to be stoichiometric, containing only the CdTe phase. After annealing, the intensity reduction takes place due to sublimation of CdTe and hence reduction in the thickness of the layer.

Copyright: © 2025 by the authors. Submitted for possible open access publication under the terms and conditions of the Creative Commons Attribution (CC BY) license (https://creativecommons.org/licenses/by/4.0/).

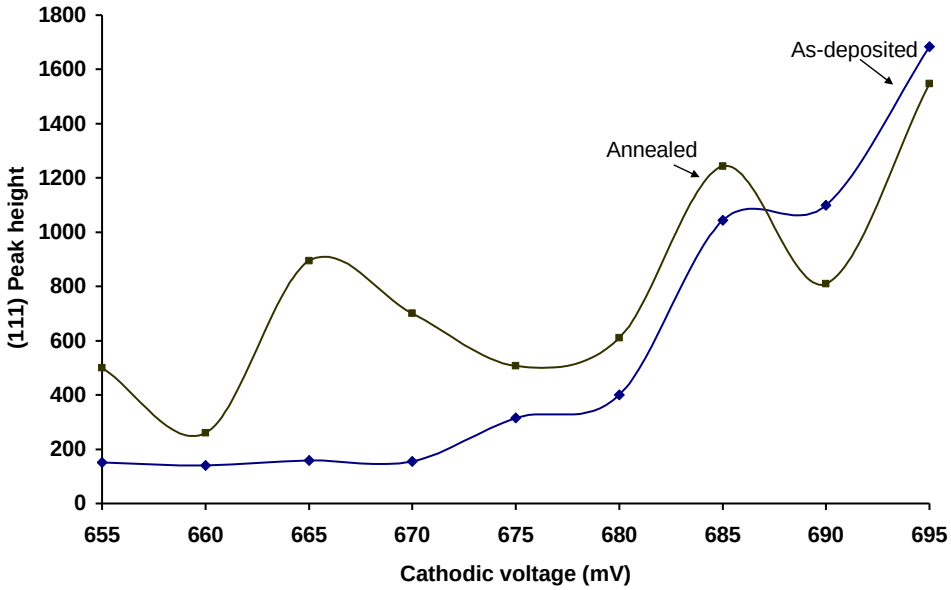

Figure 6: Variation of (111) peak height versus growth voltage for as-growth and heated CdTe films.

Conclusions

The CdTe has been electrochemically growth from aqueous solution at a range of growth voltages. The LSV was performed in order to optimize suitable voltage range. That was found from 655 to 695 mV vs. SCE. XRD technique was employed in order to characterize the CdTe materials. The highest quality layers were determined to be at growth voltage 695 mV vs SCE. it has been found; The highest intensive of (111) reflection was from (111) plane indicating a stoichiometric CdTe and an improvement of crystallinity, FHWM and Grain sie) were 0.31 deg. and 25.8 nm respectively after heat treatment, the lattice parameters of CdTe material was a=6.50 Å.

Compliance with ethical standards

Disclosure of conflict of interest

The author(s) declare that they have no conflict of interest.

References

1. Siying He, Hongting Lu, Bing Li, Jingquan Zhang, Guanggen Zeng, Lili Wu, Wei Li, Wenwu Wang, Lianghuan Feng, Materials Science in Semiconductor Processing, 67, 15 (2017) 41-45.
2. I. Repins M. Contreras, M. Romero, Y. Yan, W. Metzger, J. Li, S. Johnston, B. Egaas, C. Dehart, J. Scharf, B. E. McCandless, R. Noufi, 33rd IEEE Photovoltaic Specialists Conference May 11-16th, 2008 San Diego California.
3. X. Wu, J. C. Keane, R. G. Dhere, C. Dehart, D. S. Albin, A. Duda, T.A. Gessert, S. Asher, D. H. Levi, P. Sheldon, 17th European Photovoltaic Solar Energy Conference, 22–26th October 2001 Munich Germany.
4. Dipmala P. Sali, Nandu B. Chaure, Mateialstoday 42 (2021) 1647-1650.
5. B. D. Cullity, S. R. Stock, Elements of X-ray diffraction 3th Edition, New Jersey Prentice Hall (2001).
6. Z. Shkedi, R. L. Rod, Proc. 14th IEEE Photovoltaic Specialists Conf. IEEE New York (1980) 472-475.
7. G. C. Morris, S. K. Das, J. Solar Energy 12 (1992) 95-108.
8. N. W. Duffy, L. M. Peter, R. L. Wang, D. W. Lane, K. D. Rogers, Electrochimica Acta 45 (2000) 3355.
9. A. Kampmann, P. Cowache, J. Vedel, D. Lincot, Journal of Electroanalytical Chemistry 387 (1995) 53-64.
10. Joel Pantoja Enriquez, Xavier Mathew, Solar Energy Materials & Solar Cells 81 (2004) 363-369.
11. M. K. Rabadanov, I. A. Verin, Y. M. Ivanov, V. I. Simonov, Kristallografiya 46 (2001) 703.
12. C. Lepiller, P. Cowache, J. F. Guillemoles, N. Gibson, E. Ozsan, D. Lincot, Thin Solid Films 361-362 (2000) 118-122.

Disclaimer/Publisher's Note: The statements, opinions, and data contained in all publications are solely those of the individual author(s) and contributor(s) and not of **LJCAS** and/or the editor(s). **LJCAS** and/or the editor(s) disclaim responsibility for any injury to people or property resulting from any ideas, methods, instructions, or products referred to in the content.

Copyright: © 2025 by the authors. Submitted for possible open access publication under the terms and conditions of the Creative Commons Attribution (CC BY) license (https://creativecommons.org/licenses/by/4.0/).